Cover sheet

Author*:*

Joakim O. Blanch, BHP, Joakim.Blanch@bhp.com

Publication information:

This manuscript has not been submitted to or been published in a peer-reviewed journal. The intention is to submit an expanded version of the manuscript to a peer-reviewed journal.

Robust Q estimation using surface seismic data

J. O. Blanch

Joakim.Blanch@bhp.com

Abstract

Direct wave arrivals are the most robust signals to determine velocity and consequently they have been used for almost a century in hydrocarbon exploration. The reason is simple as the arrival time is explicitly available and provide a direct measurement of the average velocity of the sub-surface ray-path. These signals have not been extensively used to estimate attenuation or Q. One reason may be that very few robust methods have been developed to estimate Q from these signals.

The common method to estimate Q using data acquired from VSP measurements is relying on spectral ratios. This method is in general quite reliable whenever there is a signal that has a reasonably broad spectral support.

I will show how a variation on the spectral ratio method that provides equal results while more robust and how it can be adapted for surface seismic measurement.

Introduction

Attenuation of seismic energy is commonly compensated for in pre-processing (Hargreaves and Calvert, 1991). There are methodologies that are designed to generate a Q model in space from seismic data, such that attenuation effect can be compensated during migration or linearized inversion (Blanch, 1996). These methods are either straightforward FWI implementations or make use of calibrations events. The straightforward FWI implementation has a coupling with the propagation velocity model as attenuation is connected to dispersion and is sensitive to appropriate amplitude modeling, whereas the other set of methods rely on the existence of an appropriate calibration event. If no such event exists, the method is not applicable. Another set of methods

make use of instantaneous frequency estimates in order to generate an objective function (Chen et al., 2018, Dutta and Schuster, 2016, He and Cai, 2012, Hu et al., 2011).

A reasonably robust method used for VSP (vertical seismic profiling) is to generate spectral ratios at different recording stations (White, 1992). The method still requires a fairly stable signal spectrum in order to correctly estimate the slope of the spectra. Here, I will propose an objective function for propagating waves that maintain the robustness of the spectral ratio method, but does not require the estimation of a slope, and is applicable to surface seismic data. The objective function will be applied to surface seismic through the use of the adjoint state method. As such the objective function can be used with both ray based and full waveform propagators. I will show the application of the objective function in a synthetic example with a simple velocity model and ray propagators.

Objective function

I will show an objective function based on spectral slope comparisons and then show an objective function that has the same behavior but does not use the estimate of a slope and that is independent of absolute values of the spectra. An objective function J based on slope for a calibration/source point and a receiver point is simply,

$$J(Q) = \frac{1}{2}\int_{fa}^{fb}(k_m - k_d)^2\,df \tag{1}$$

$$k = average\ slope\left(ln\left(\frac{S(f)_r}{S(f)_c}\right)\right) \tag{2}$$

f is frequency, S_r is the amplitude spectrum of a recorded signal at a recording point, and S_c is the amplitude spectrum of the signal at a calibration point, see Figures 1 and 2. The subscript c and r refers to the signal at the calibration point and recording point respectively, and the subscripts d and m refers to recorded and modeled data respectively.

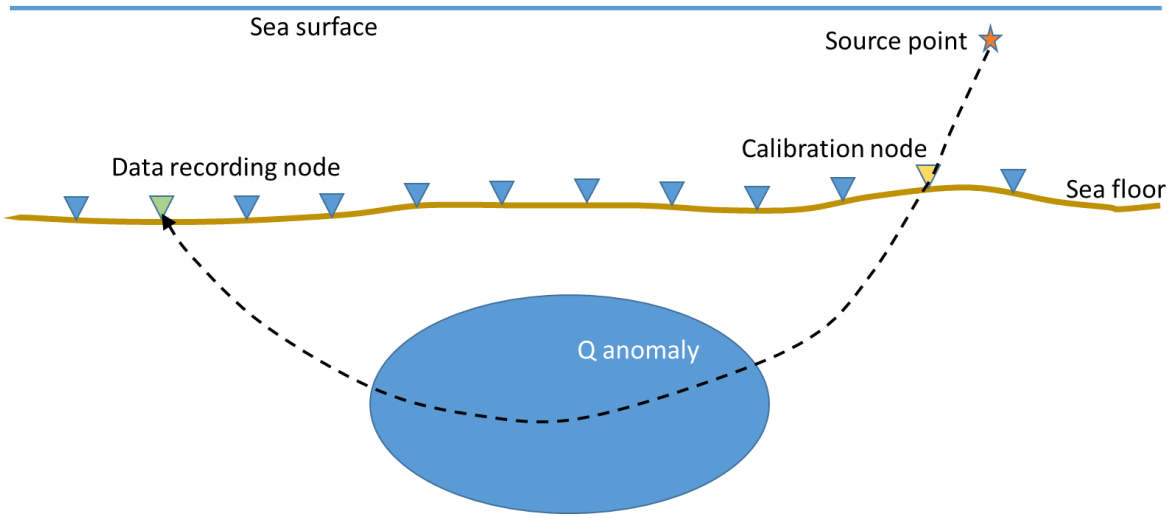

Figure 1 shows the measurement points of the different signals using an OBS acquisition for direct arrivals.

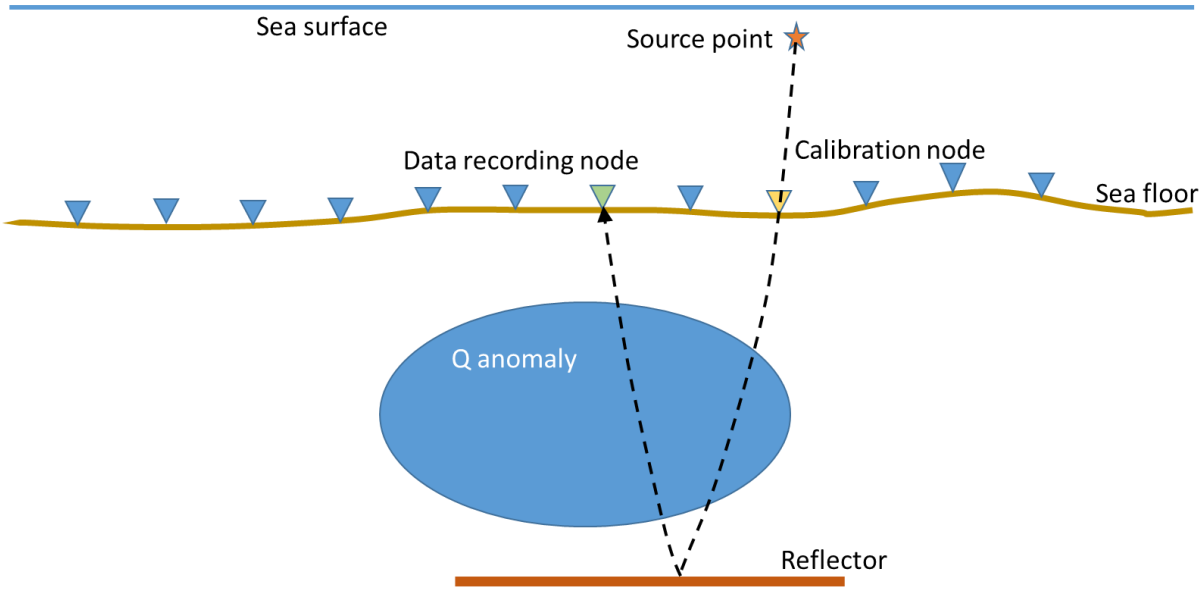

Figure 2 shows measurement the points of the different signals using an OBS acquisition for reflected arrivals. In this case, reflected arrivals in addition to direct must be modeled.

The calibration spectra can also be estimated from near field recordings or other means. The slope k_d is estimated from the measured data, and the slope k_m is estimated from the modeled data. In the example in Figure 3, the slope is estimated using regression. As the spectra are normalized, they do not need to be exactly the same for the objective function to work. This objective function is

entirely based on the constant Q assumption and assuming that the spectra have reasonable support in order to estimate a stable slop. Another objective function that could be used is:

$$J(Q) = \frac{1}{2}\int_{fa}^{fb}\left(\frac{d}{df}\,ln\left(\frac{\left(\frac{S(f)_{mr}}{S(f)_{mc}}\right)}{\left(\frac{S(f)_{dr}}{S(f)_{dc}}\right)}\right)\right)^2 df \qquad (3)$$

This objective can be split over several intervals where the signal has support. It requires that the slope between the two ratios is constant. This is for instance true for a constant Q medium and thus be equivalent to the objective function in equations 1 and 2. One benefit is that the absolute value does not have to match, just that the ratio is constant over the measured frequency range. Another one is that the first is assuming a constant Q model, whereas the second in theory could handle any type of Q versus frequency relationship. It is also a little more straightforward to implement than estimating slopes. The comparison between the two objective functions are shown in Figure 3. By normalizing the objective functions, it is clear that they are identical for the simple test example.

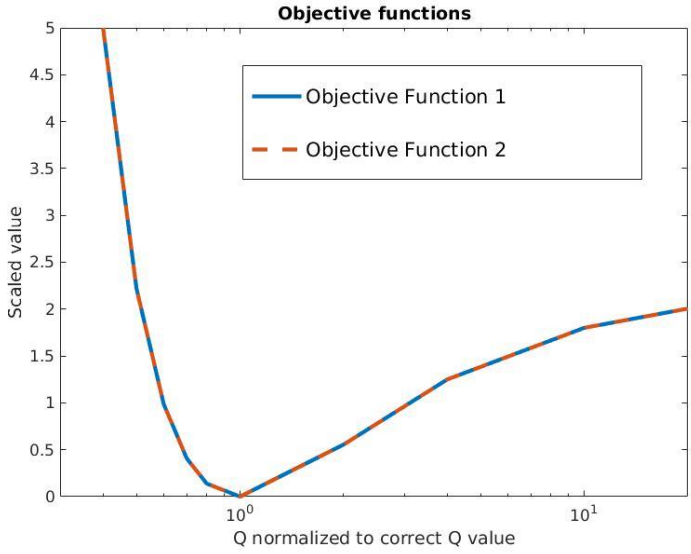

Figure 3 shows the two objective that have been scaled to have the same maximum value. As is evident the objective functions are the same after scaling. The objective function is not convex for very large Q values, but appears to have the correct slope

and no clear local minima. Objective function 1 corresponds to Equation 1 and 2 and Objective function 2 corresponds to Equation 3. The test scenario is modeled to be similar to Figure 1 with one ray going through a region with a small Q value. To generate the objective function the Q value in the region was varied from very high attenuation to essentially no attenuation.

It is clear that the shape of the objective functions in Figure 3 is reminiscent of an inverse. The abscissa has been in inverted in Figure 4 as compared to Figure 3 and the function in Figure 4 looks clearly convex, which is investigated below.

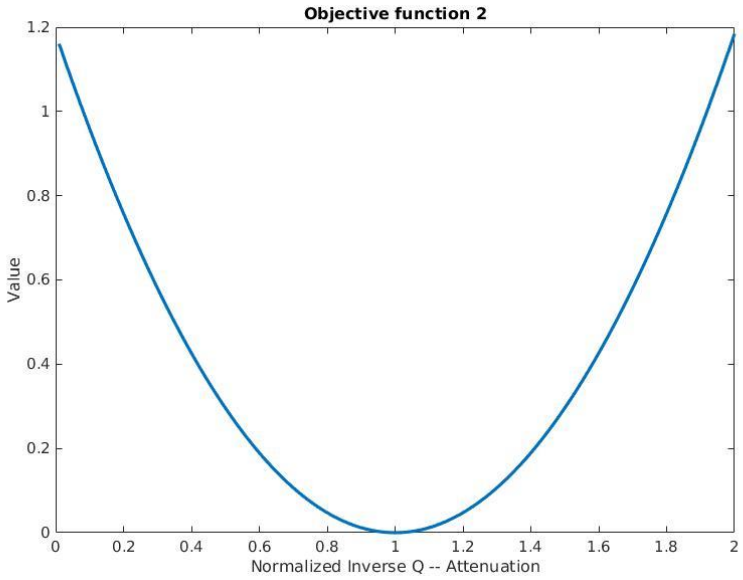

Figure 4 shows the objective function from Equation plotted against the inverse of Q. Plotting the objective function in this manner seems to suggest it is convex with no local minima for the test example. Q ranges from a value several magnitudes larger than the correct value to half the correct value. The correct Q value is at the abscissa value of 1 in the graph.

Thus optimizing the objective function with respect to the inverse of Q should possibly yield a convex objective function, which would enable stable and fast convergence.

Gradient calculations

Robust Q estimation using surface seismic data

In order to use the objective function for optimization using an algorithm that takes of advantage of its apparently convex nature it is necessary to compute the gradient of the function. The gradient naturally depends on the forward modeling algorithm for the wave propagation. The gradient can be viewed to be comprised of two parts, one part that is related to the objective itself and one part that is dependent on the forward modeling algorithm. For a "least squares objective function" the first part is trivial which is likely why it is such a popular choice. I will derive one gradient that is based on ray propagation and one, which is based on full wave-form modeling as examples. From these two examples, it should be easy for anyone to apply the objective any preferred forward modeling algorithm. The first part of the gradient is quite straight forward as is shown in Equation 4.

$$\delta J(Q) = \int_{f_a}^{f_b} \left(\frac{d}{df} \ln \left(\frac{\left(\frac{S(f)_{mr}}{S(f)_{mc}}\right)}{\left(\frac{S(f)_{dr}}{S(f)_{dc}}\right)} \right) \right) \left(\frac{d}{df} \frac{\delta S(f)_{mr}}{S(f)_{mr}} \right) df \tag{4}$$

$$\delta S(f) = \frac{\partial S(f)}{\partial \alpha} \delta \alpha \tag{5}$$

The quantity α is proportional to the inverse of Q in order to try to achieve a well-posed objective function. The variation of the measured spectrum depends on the modeling methodology, but the part of the gradient that has been derived at this point could be seen as the source for any adjoint partial differential equation.

Ray propagator gradient:

In the case of a forward model based on a ray propagator the forward model is simply to sum attenuation values along a ray path based on the constant Q model from White, 1992,

$$S(f)_{mr} = e^{-\int_{\gamma a}^{\gamma b} \omega \alpha(\gamma)\, d\gamma} = e^{-\int_{\gamma a}^{\gamma b} 2\pi f \alpha(\gamma)\, d\gamma} \tag{6}$$

Where ω is the angular frequency. The integration is over the ray path γ. This forward model implicitly assume the same ray path for different frequencies. This is however only true to first approximation as the attenuating medium is dispersive. The variation of the propagator is

$$\delta S(f)_{mr} = -e^{-\int_{\gamma a}^{\gamma b} \omega \alpha(\gamma)\, d\gamma} \int_{\gamma a}^{\gamma b} \omega\, \delta\alpha(\gamma)\, d\gamma = -S(f)_{mr}\, 2\pi f \int_{\gamma a}^{\gamma b} \delta\alpha(\gamma)\, d\gamma \tag{7}$$

The last integral is a scalar product between the variation in attenuation and the identity

$$\int_{\gamma_a}^{\gamma_b} \delta\alpha(\gamma)\, d\gamma \;\stackrel{\text{def}}{=}\; (\mathbf{1}, \delta\alpha) \tag{8}$$

Hence, the adjoint of **1** distributes the gradient value evenly across the ray. The gradient is thus simply the value of the integrals spread along the ray path.

Full wave propagator gradient:

The full wave propagator example is based on a viscoacoustic equation using relaxation mechanisms to approximate a realistic medium (Blanch, 1996).

$$\begin{cases} p_{,t} = K(1+n\alpha)\,\overline{\nabla}\cdot\overline{v} + K\alpha\sum_i r_i \\ r_{i,t} = -\frac{1}{\tau_{\sigma i}}\left(r_i + W_i\overline{\nabla}\cdot\overline{v}\right) \\ \overline{v}_{,t} = \frac{1}{\rho}\overline{\nabla}p \end{cases} \tag{9}$$

Where p and v are pressure and velocity, and there are n relaxation mechanisms r_i. K is the bulk modulus and ρ is the density. The $\tau_{\sigma i}$ are relaxation times related to the different relaxation mechanisms, and the W_i are weights that determine the behavior versus frequency and if they are all equal to one, the system will approximate a constant Q versus frequency with appropriately chosen relaxation times. The system needs source terms, which could be added to any of the individual equations. Linearizing the equation or equivalently applying the Born approximation (e.g. $p = p_0 + \delta p$) yields

$$\begin{cases} p_{0,t} = K_0\,(1+n\alpha)\overline{\nabla}\cdot\overline{v}_0 + K_0\alpha_0\sum_i r_{0i} \\ r_{0i,t} = -\frac{1}{\tau_{\sigma i}}\left(r_{0i} + W_i\overline{\nabla}\cdot\overline{v}_0\right) \\ \overline{v}_{0,t} = \frac{1}{\rho_0}\overline{\nabla}p_0 \end{cases} \tag{10}$$

$$\begin{cases} \delta p_{,t} = K_0\,(1+n\alpha)\,\overline{\nabla}\cdot\delta\overline{v} + K_0\alpha_0\sum_i \delta r_i + K_0\delta\alpha\,(n\overline{\nabla}\cdot\overline{v}_0 + \sum_i r_{0i}) \\ \delta r_{i,t} = -\frac{1}{\tau_{\sigma i}}\left(\delta r_i + W_i\overline{\nabla}\cdot\delta\overline{v}\right) \\ \delta\overline{v}_{,t} = \frac{1}{\rho_0}\overline{\nabla}\delta p \end{cases} \tag{11}$$

Both systems are governed by the same PDE except that there is a source term for the linear system. Hence, it could be represented with an operator A_0 that includes all differential operator as well as parameters.

$$A_0 \bar{u}_0 = \bar{f} \tag{12}$$

$$A_0 \delta\bar{u} = \begin{bmatrix} K_0 \delta\alpha \left(n\bar{\nabla} \cdot \bar{v}_0 + \sum_i r_{0i}\right) \\ \vdots \\ 0 \end{bmatrix} \tag{13}$$

where a source term f has been added and u is the combination of all fields. The signal s is for instance the pressure field sampled at a location x_r with a source term at a location x_s.

$$s(t) = p(t, x_r, x_s) \tag{14}$$

The adjoint PDE is derived through the adjoint state method and is

$$A_0^* \bar{q} = \bar{\sigma} \tag{15}$$

$$\Delta\alpha = \int_0^T q_1 \left(K_0 n\bar{\nabla} \cdot \bar{v}_0 + \sum_i r_{0i}\right) dt \tag{16}$$

Where q_1 is the first component of the vector. The source is s is derived from the definition of $S(f)$.

The spectrum $S(f)$ is the power of the Fourier transform of the signal $s(t)$.

$$S(f) = \sqrt{\hat{S}^*(f)\,\hat{S}(f)} \tag{17}$$

$$\hat{S}(f) = \frac{1}{\sqrt{2\pi}} \int_{-\infty}^{\infty} s(t)\, e^{-j2\pi f t} dt \stackrel{\text{def}}{=} \mathrm{F}[s(t)] \tag{18}$$

The operator F symbolizes the Fourier transform and will be convenient to use for the adjoint. Hence the variation of $S(t)$ in equation 4 is

$$\delta\hat{S}(f) = \frac{1}{S(f)} F[\delta s(t)] \tag{19}$$

Which combined with equation 4 yields,

$$\delta J(Q) = F^* \left[\int_{fa}^{fb} \left(\frac{d}{df} ln \left(\frac{\left(\frac{S(f)_{mr}}{S(f)_{mc}}\right)}{\left(\frac{S(f)_{dr}}{S(f)_{dc}}\right)} \right) \left(\frac{d}{df} \frac{1}{S^2(f)_{mr}} \right) df \right] \delta s(t) \tag{20}$$

The argument to the adjoint operator *F** is constant and it is simply passed through as the *F** is the inverse Fourier transform. Thus the source in equation 14 is,

$$\overline{\sigma} = \begin{bmatrix} Cs(t) \\ \vdots \\ 0 \end{bmatrix} \tag{21}$$

C is the constant obtained by carrying out the integration over *f* in equation 19, and *s(t)* is the recorded wavefield.

Extension to several sources and receivers:

The derivations above are suitable for one source point and potentially several receivers for the full wave propagator. The extension to several sources, and for the ray propagator receivers, is straightforward. The combined objective function is just the sum of the individual objective as is the gradient.

$$J_{Tot}(Q) = \sum_{Sr,Rc} J_{Sr,Rc}(Q) \tag{22}$$

$$\frac{\partial J_{Tot}(Q)}{\partial \alpha} = \sum_{Sr,Rc} \frac{\partial\ J_{Sr,Rc}(Q)}{\partial \alpha} \tag{23}$$

Convexity of objective function

For a constant Q media represented using the ray-propagator described above the objective function in equation 3 is,

$$J(Q) = \frac{1}{2}\int_{f_a}^{f_b} \left(\frac{d}{df}\, ln\left(\frac{e^{-\int_{\gamma_a}^{\gamma_b} 2\pi f \alpha_m(\gamma)\, d\gamma}}{e^{-\int_{\gamma_a}^{\gamma_b} 2\pi f \alpha_f(\gamma)\, d\gamma}} \right) \right)^2 df \tag{24}$$

assuming the calibration spectra are the same. Applying the logarithmic to the exponentials yields,

$$J(Q) = \frac{1}{2}\int_{f_a}^{f_b} \left(\frac{d}{df} 2\pi f \int_{\gamma_a}^{\gamma_b} (\alpha_f(\gamma) - \alpha_m(\gamma))\, d\gamma \right)^2 df \tag{25}$$

$$J(Q) = \frac{1}{2}\int_{f_a}^{f_b} \left(2\pi \int_{\gamma_a}^{\gamma_b} (\alpha_f(\gamma) - \alpha_m(\gamma))\, d\gamma \right)^2 df \tag{26}$$

Using this expression, it is straightforward to get the second derivative with respect to α_m,

$$\frac{\partial J}{\partial \alpha_m}(Q) = \int_{f_a}^{f_b} 4\pi^2 \int_{\gamma_a}^{\gamma_b} d\gamma \int_{\gamma_a}^{\gamma_b} (\alpha_m(\gamma) - \alpha_r(\gamma))\, d\gamma\, df \tag{27}$$

and the second derivative,

$$\frac{\partial^2 J}{\partial \alpha_m^2}(Q) = \int_{f_a}^{f_b} 4\pi^2 \left(\int_{\gamma_a}^{\gamma_b} d\gamma \right)^2 df > 0 \tag{28}$$

for any finite interval on f and γ.

Hence, the objective function is convex for a constant Q model to first approximation.

Example application

The example is built using a ray propagator and a simple gradient velocity model. The ray solution can be found analytically and is described by Stovas and Alkhalifah 2014. The velocity at the source and recording surface is 2500 m/s and increases with a gradient of 2 s^{-1}. Sources are placed at 100 m intervals and receivers follow sources at 50 m spacing with offsets ranging from 200 m to 5.5 km. The source has support in the band 5 to 80 Hz. The true attenuation model is shown in Figure 5. The background Q is 500 and the region of anomalous Q is 150.

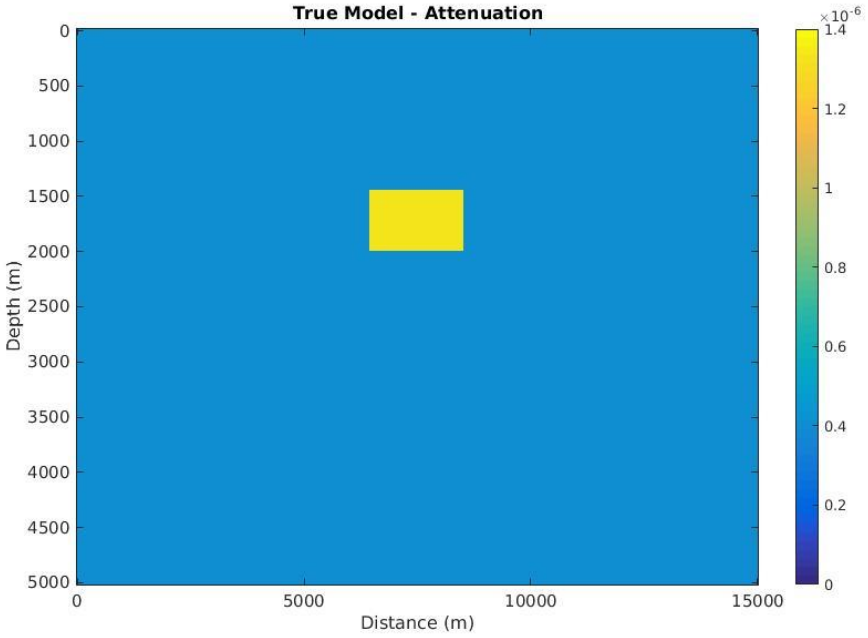

Figure 5. True Q model. Value shown is proportional to the inverse of Q.

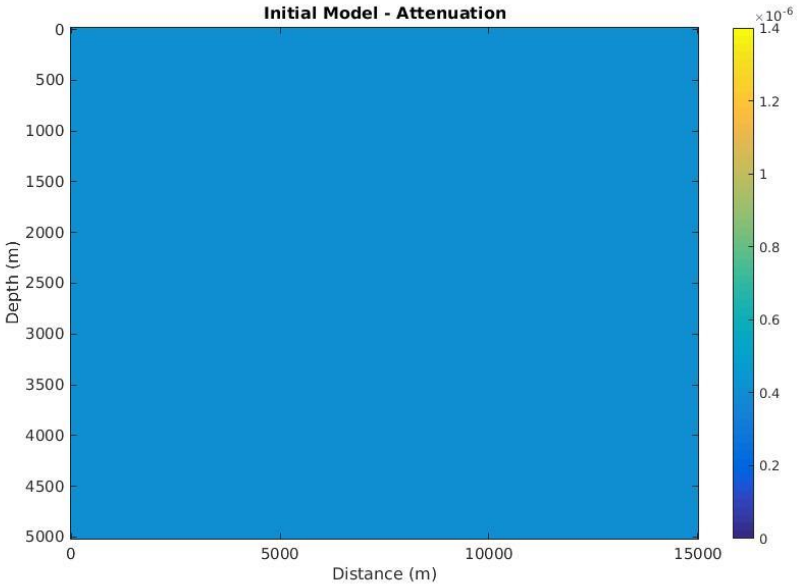

Figure 6. Inital Q model. Value shown is proportional to the inverse of Q.

The initial model is shown in Figure 6 and is the background Q value of 500 throughout. The first gradient calculation is shown in Figure 7. It indicates the ray coverage of the area with the lower Q.

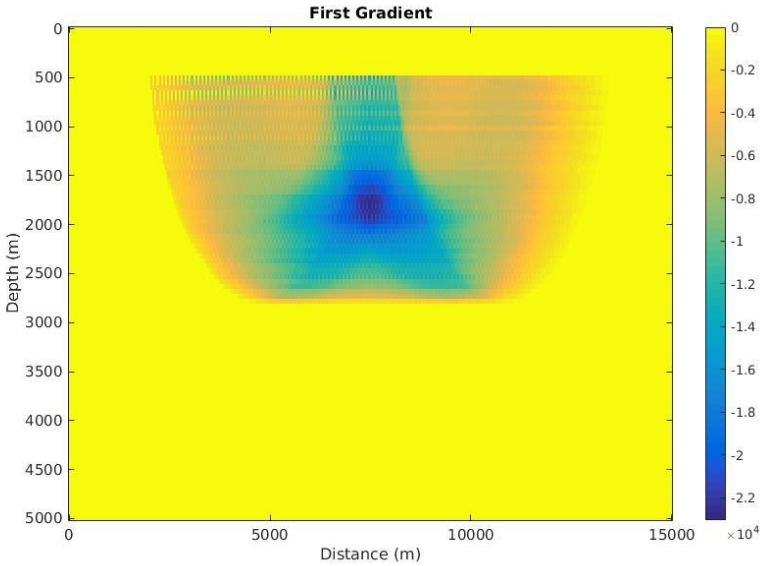

Figure 7. First gradient. Value shown is proportional to the inverse of Q.

Using the gradient with a simple line search results in the convergence of the objective function and the norm of the gradient shown in Figures 8 and 9. The inversion was run for 8 iterations when counting the initial value as iteration 1.

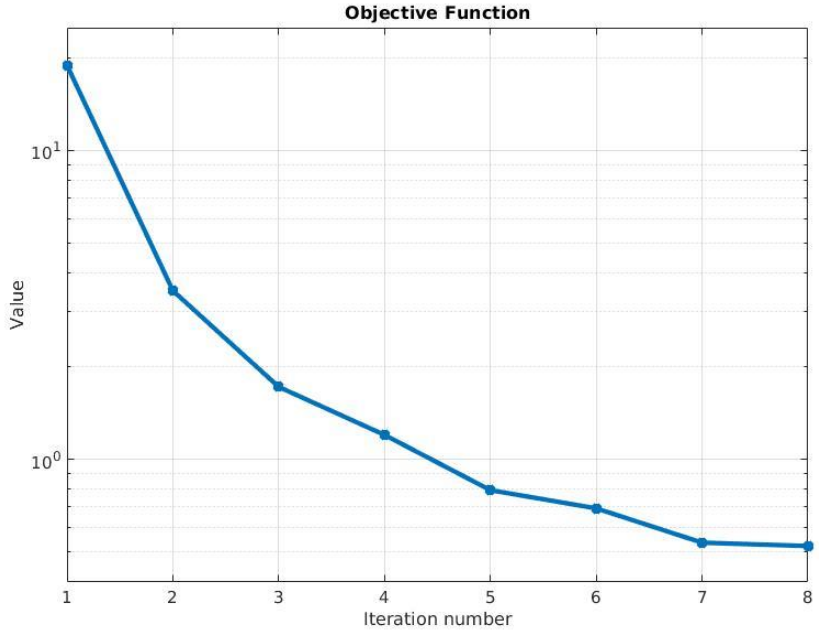

Figure 8. Convergence of objective function

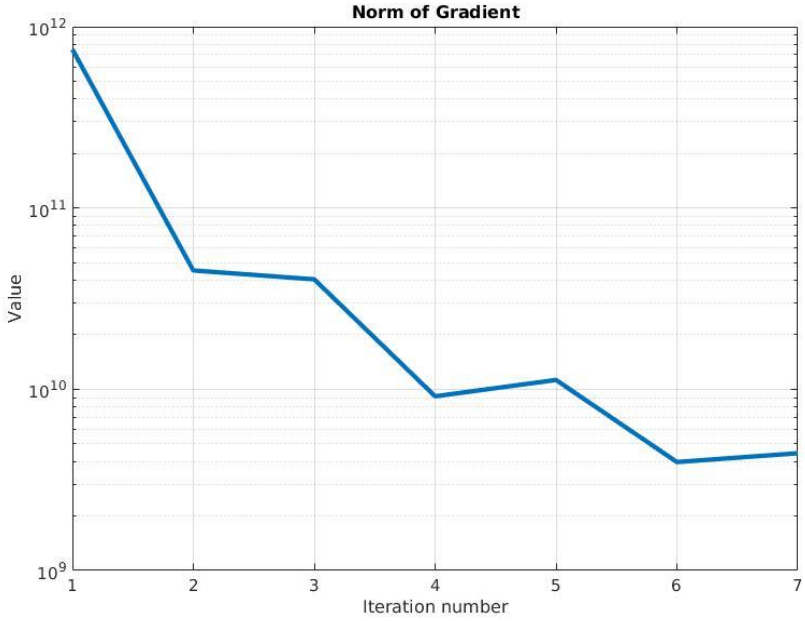

Figure 9. Convergence of the norm of the gradient

The objective function shows a steady convergence whereas the gradient at times is slightly larger than the preceding value. The resulting Q model is shown in Figure 10. The inverted model has largely captured the value and shape of the anomaly. The difference is due to limited bandwidth and ray coverage.

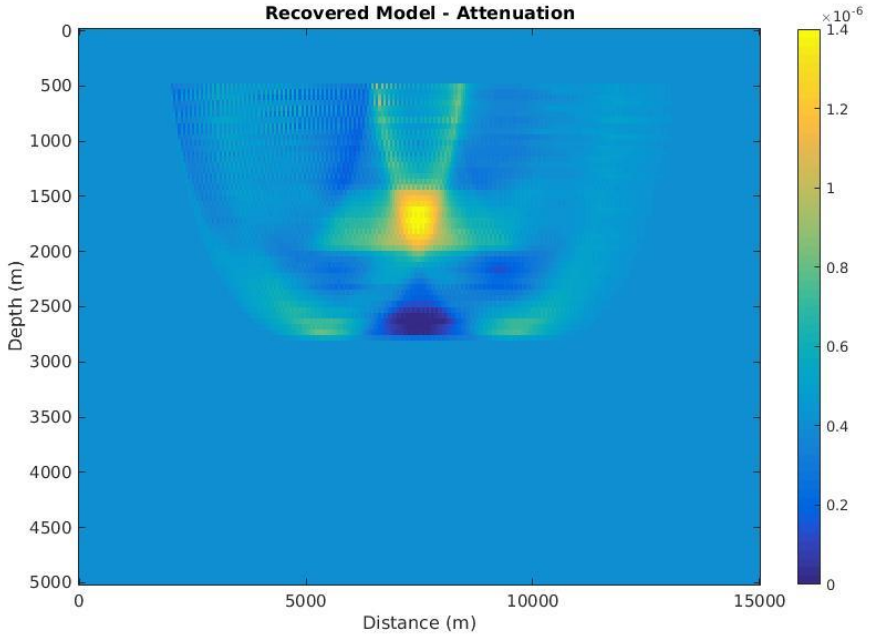

Figure 10. Attenuation model recovered after 8 iterations. Value shown is proportional to the inverse of Q.

Implementation considerations

The range of integration over frequency $[f_a,f_b]$ in the objective function can be broken into several ranges where the measured signal has support i.e., integration over the range $[f_1,f_2]$ and $[f_3,f_4]$ for instance.

The objective functions use a calibration spectrum that is dependent on the particular ray path. However, if the source signature is relatively stable from source point to source point, it should suffice to calibrate with the source spectrum, making this calibration spectrum constant for all receiver positions. The modeled source could also be constructed such that it is the same as the source spectrum, and thus removing the calibration spectra from the objection function.

The objective function above is still constructed such that it is necessary to keep track of the propagating wave paths through the received spectra. Neglecting multi-arrivals at the same time at a receiver location, it is possible to create an objective function dependent in time, such that several wave-paths can be taken care of without monitoring the actual wave paths. The objective function is made dependent on time by windowing the operator

$$F[s(t)] = \frac{1}{\sqrt{2\pi}} \int_{-\infty}^{\infty} s(t) e^{-j2\pi f t} dt \qquad (29)$$

$$F[s(t)] = \frac{1}{\sqrt{2\pi}} \int_{-\infty}^{\infty} Win(t-\tau)s(t)e^{-j2\pi ft}dt \qquad (30)$$

The window can be a cosine taper or some other window function centered on zero. This will make the objective function $J(\alpha)$ a function of time τ, $J(\alpha, \tau)$, and the constant C in equation 21 dependent on time t, $C(t)$. This can be done for both the ray- and full wave-propagator. It is important to note that the adjoint of the operator F now also contains the window function.

Discussion and conclusions

It is possible to build an objective function for Q estimation that behaves as slope based objective function for a constant Q medium that does not rely on a calibration event or would suffer through mixing with other parameters such as velocity. The objective function can be applied for media that is not governed by a constant Q as well. The objective function can be applied to ray propagator or full-wave modeling methods. It is straightforward to show that the objective function is convex, if it is function of a quantity that is the inverse of Q. A constant Q model example based on constant Q and a ray propagator shows that inversion based on the objective function quickly converges toward the correct solution. The objective function can easily be extended from direct arrivals to reflected arrivals. Furthermore, the extended version can handle wave arrivals through volumes with different Q values.

The methodology relies on existence of a reliable velocity model. Hence, it is necessary to have a good velocity model prior to Q determination, and update the velocity model again after the Q has been determined.

Acknowledgments

The author wish to thank BHP for permission to publish the results.

References

Blanch, J. O., 1996, "A study of viscous effects in seismic modeling, imaging, and inversion: Methodology, computational aspects, and sensitivity", 1996, PhD thesis, Rice University

Chen, Y., G. Dutta, G. T. Schuster, "Image-Domain Q Inversion", 2018, SEG, Expanded Abstracts, 4121-4125, DOI http://dx.doi.org/10.1190/ segam2018-2997203.1

Dutta, G., G. T. Schuster, "Skeletonized wave-equation inversion for Q", 2016, SEG, Expanded Abstracts, 3618-3622.

Hargreaves, N. D., A. J., Calvert, "Inverse Q filtering by Fourier transform", 1991, Geophysics, **56**, 519-527

He, Y., J. Cai, "Q tomography towards true amplitude image and improve sub-karst image", 2012, Society of exploration geophysicists annual meeting, DOI http://dx.doi.org/10.1190/segam2012-1220.1

Hu, W., J. Liu, L. Bear, C. Marcinkovich, 2011, "A robust and accurate seismic attenuation tomography algorithm", SEG, Expanded Abstracts", 2727-2731.

Stovas, A., T. Alkhalifah, "Analytical approximations of diving-wave imaging in constant-gradient medium", 2014, Geophysics, **79**, S131-S140

White, R. E., "The accuracy of estimating Q from seismic data", 1992, Geophysics, **57**, 1508-1511